Available online at www.sciencedirect.com
ScienceDirect
Journal of the European Ceramic Society 31 (2011) 903–911
www.elsevier.com/locate/jeurceramsoc

Novel electrically conductive α–β SiAlON/TiCN composites

Erhan Ayas, Alpagut Kara *

Department of Materials Science & Engineering, Anadolu University, Eskisehir 26555, Turkey

Received 2 August 2010; received in revised form 9 November 2010; accepted 25 November 2010
Available online 24 December 2010

Abstract

Electrically conductive α–β SiAlON/TiCN composites were produced in the form of a segregated network in a ceramic matrix structure. A continuous 3D network of conductive TiCN particles was successfully achieved by mechanically coating spray-dried SiAlON granules with varying amounts of nano sized TiCN (0–10 vol.%) particles. For comparison, the same SiAlON matrix was incorporated with 25 vol.% micron sized TiCN particles to give a particle reinforced composite. Densification, together with mechanical and electrical properties of the composites produced were discussed in terms of conventional and novel approach. Fully dense composites were obtained by gas pressure sintering (GPS) under a nitrogen pressure of 100 bar at a peak temperature of 1990 °C. The electrical resistivity of the SiAlON (1×10^{13} Ω m) matrix material was drastically reduced with the addition of only 5 vol.% TiCN (18×10^{-4} Ω m) to the composites prepared by the coating method.

Keywords: α–β SiAlON; TiCN; Dry mixing; Electrical conductivity; Gas pressure sintering (GPS)

1. Introduction

Al_2O_3, ZrO_2, Si_3N_4 and the SiAlON's are the most important and applicable commercial structural ceramics owing to their outstanding properties. Among these, Si_3N_4 and the SiAlON's are in a particular class of materials due to their attractive combination of high mechanical and thermal properties which they possess both at room and high temperature. These materials are generally used for cutting tools, mechanical seals, bearings, heat exchangers and components for heat engines usually in the form of a monolithic material.[1] For further improvement of the properties, several reinforcement materials have been successfully incorporated into Si_3N_4 and SiAlON matrix materials.[2] With this composite approach, new possibilities have developed to broaden the application areas of these materials because of their new and different properties. One of the most important features is electrical conductivity, which has allowed the use of these materials in electrical applications such as glow plugs and heaters.[1] Furthermore, this feature allows the possibility of producing complex shaped parts by employing the Electro Discharge Machining (EDM) process.[3–5]

In order to provide electrical conductivity, addition of conductive secondary phases like TiN,[6–9] SiC,[10–12] TaN,[13] $MoSi_2$,[14–16] Ti(C, N)[17,18] and TiB_2[19] in the composite approach has been extensively investigated. However, to achieve the desired electrical conductivity value, high amounts (30–40 vol.%) of such secondary phases must be introduced into the matrix material. On the other hand, such large additions usually lead to the degradation of some of the important properties of the matrix material. Moreover, insufficient dispersion of secondary phases and the chemical incompatibility between the matrix and reinforcement material is the most common problem encountered. The densification of this type of composites is a difficult task to accomplish. Hot pressing (HP) and hot isostatic pressing (HIP) are generally preferred for commercial products. However, materials produced using these techniques invariably need to be subjected to secondary machining processes, which is costly and time consuming. To overcome above mentioned problems, the amount of secondary phase addition must be kept as low as possible. For this purpose, techniques which promote in situ formation of conductive particles through chemical precursors or direct incorporation of convertible oxide additives have also been studied.[20–22] However, the complexity of chemical processes and the unwanted grain growth of in situ formed phases, even at fast heating rates (such as spark plasma sintering), negatively affects the electrical conductivity and mechanical properties of the matrix material.

* Corresponding author. Tel.: +90 222 321 35 50x6584; fax: +90 222 323 95 01.
E-mail address: akara@anadolu.edu.tr (A. Kara).

0955-2219/$ – see front matter © 2010 Elsevier Ltd. All rights reserved.
doi:10.1016/j.jeurceramsoc.2010.11.026

The segregated network concept, which is a commonly used method in polymer matrix composites (PMC) has been found to be an effective means of achieving high electrical conductivity with a very low conductive phase content.[23–25] In this concept, insulating and conductive powders with different particle sizes are mixed together under specific conditions. Mostly, the filler conductive particles are not uniformly distributed on a micro scale but are retained at the interface between grains of the insulating matrix phase, forming a conductive network. In such type of composites, electrical conductivity increases only after a critical value of filler concentration, known as the percolation threshold. As the filler content is increased just beyond the percolation threshold; the conductivity value dramatically increases by several orders of magnitude.[26,27] Hence, it was emphasized that the perfect composite structure must include spherical shaped particles in order to promote a continuous network of conductive phase.[28] For this purpose, one can predict that coating a spherical particle with a conductive phase can be an innovative choice.

Considering the overall approaches, spray drying can be an effective way to produce granules in a spherical shape. In the pharmaceutical and food industry, the use of granules, and the subsequent coating of their surfaces is a common approach.[29,30] In order to modify the diffusion rate of drugs or foods, a core shell structure is produced by coating granules with different kinds of relevant substances. The coating process is a relatively wet chemical process and generally performed in a fluidized bed reactor.[31] Dry coating using mechanical methods which exclude any liquid solvent or binder solution can, however, be preferred in order to save time, energy, number of additives, process steps and consequently to reduce the cost of the whole process. Dry-coating appears to be an interesting way to create new composite materials in various application areas. Granules having a relatively large size (host particles, 1–500 μm) can be mechanically coated with fine particles (guest particles, 0.1–50 μm) in order to create new functionality or to improve their initial characteristics.

In this work, SiAlON based granules with a fixed composition were prepared by spray drying and coated with nano TiCN particles in varying amounts using a dry mixing process. Densification behavior, together with the electrical and mechanical properties of the composites were compared with a conventional TiCN particle reinforced SiAlON matrix of the same composite.

2. Materials and methods

2.1. Preparation of TiCN coated SiAlON composites (SNC)

Spray dried SiAlON granules were supplied by MDA Advanced Ceramics Ltd. (Eskisehir/Turkey). The composition was designed to obtain 25% α–SiAlON/75% β-SiAlON in the final product. The constitution of the composition and the detailed preparation route are given elsewhere.[32] α–β SiAlON composition was prepared by using starting powders of 89.4 wt% Si_3N_4 (SN-E10, Ube Industries Ltd., Japan), 5.4 wt% AlN (HC Starck GmbH, Germany), 2.5 wt% Al_2O_3 (Sumitomo, Japan), 4.73 wt% Y_2O_3 (Shin Etsu Chemical Co., Ltd., Japan), 0.4 wt% Sm_2O_3 (Sigma–Aldrich, Germany) and 0.12 wt% $CaCO_3$ (Riedel-de Haën, Germany). The powders were mixed through attrition milling with de-ionized water as liquid media and Si_3N_4 grinding balls for 2 h in a polyamide container. The slurry was then dried in a spray drier (Nubilosa, Germany) in order to obtain spherical granules of around 100 μm in diameter, under suitable conditions (Fig. 1a and b). $TiC_{0.7}N_{0.3}$ (<150 nm, Sigma–Aldrich) powder was used as the coating material. Appropriate amounts of SiAlON granules and TiCN powder (0, 2.5, 5, 7.5 and 10 vol.%) were weighted and dry mixed in a polyethylene bottle without any liquid and grinding media. The mixing process was carried out under RT conditions in a classical ball mill device with a rotational speed of 30 rpm/min.

For comparison, a 25 vol.% TiCN particle reinforced SiAlON composite was also prepared from SN and $TiC_{0.5}N_{0.5}$ powder (H.C. Starck, Grade B, Germany). The weighted powders were planetary ball milled (Pulverisette 6 Fritsch, Germany) in a Si_3N_4 jar with Si_3N_4 balls for 2 h in isopropanol. Then, the slurry was dried using a rotary evaporator and sieved in order to break agglomerates.

2.2. Shaping and gas pressure sintering (GPS)

Both powders were dry pressed with a computer controlled automatic uniaxial press (Dorst, Germany) under 50 kN load. Sintering of the pellets was carried out in a h-BN crucible using a GPS furnace (FCT Systeme GmbH, Germany), capable of operating at temperatures of up to 2000 °C in an inert atmosphere of up to 10 MPa pressure. A two-stage sintering schedule was employed. The first stage of sintering was achieved at 1940 °C for 60 min under a nitrogen gas pressure of 0.2–0.5 MPa. In the second stage, both the peak temperature and gas pressure were raised to 1990 °C and 10 MPa, respectively, for the same soaking time. The heating and cooling rates were kept at 10 °C/min.

2.3. Characterisation

Relative densities of the samples were measured with distilled water at room temperature by the Archimedes method. Phase identification was performed on ground powder samples using XRD (Rigaku Rint 2200-Japan) with Ni-filtered Cu Kα radiation of wavelength 1.5418 Å. Intensities of the (1 0 2) and (2 1 0) peaks of the α-SiAlON phase and the (1 0 1) and (2 1 0) peaks of the β-SiAlON phase were used for quantitative estimation of the α:β phase ratio.[33] Vickers hardness (Hv_{10}) from the polished surfaces of the sintered samples was measured by using an indenter (Emco-Test, M1C, Germany) with a load of 10 kg. The fracture toughness (K_{IC}) of the samples was evaluated from the radial cracks formed during the indentation test using the equation given below[34]:

$$K_{IC}\Phi = 0.15 H_v \sqrt{ak}\left(\frac{c}{a}\right)^{-3./2} \quad (1)$$

where K_{IC}, H_v are the toughness and hardness of the material; a and c are the impression radius and the crack length in the diagonal direction of the indent, Φ and k are the constraint factor ($\Phi = 3$) and the surface constant ($k = 2.6$). Electrical resistivity

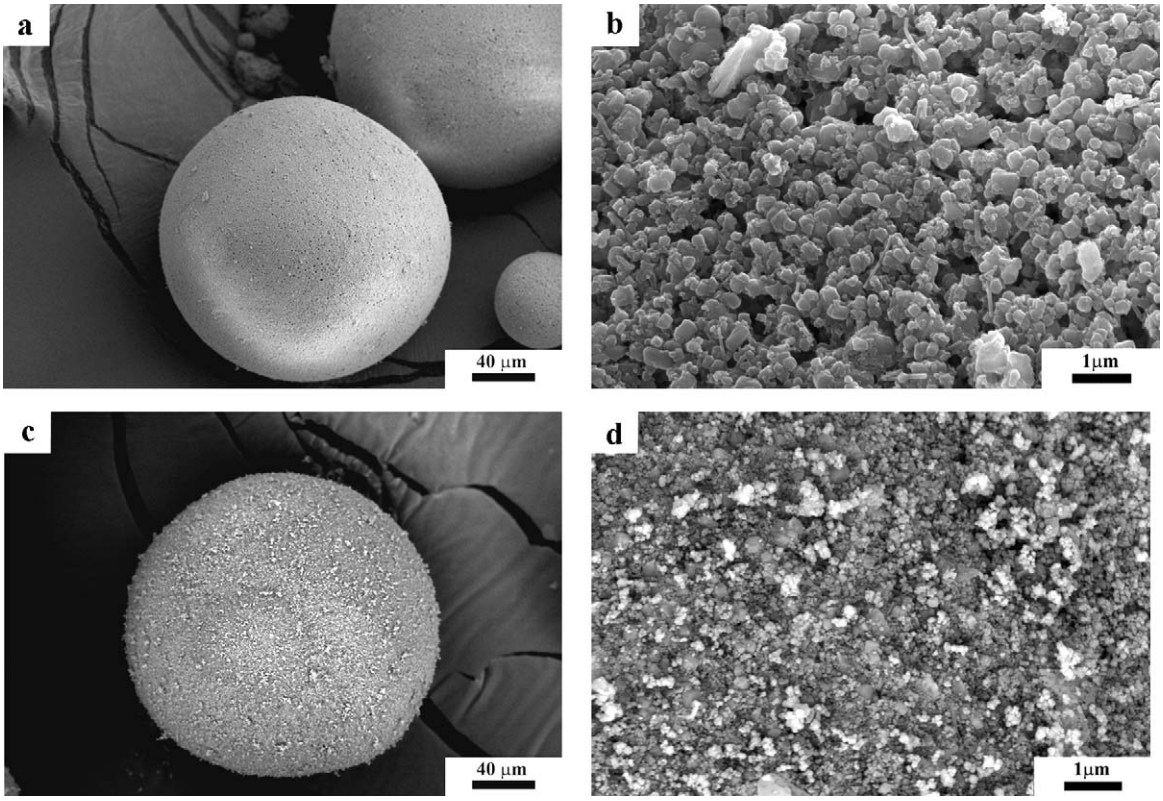

Fig. 1. SEM images of the surfaces of SiAlON based granules before and after coating with nano $TiC_{0.7}N_{0.3}$ particles. (a) Uncoated granule surface – low mag. (b) Uncoated granule surface – high mag. (c) 5 vol.% $TiC_{0.7}N_{0.3}$ coated granule surface – low mag. (d) 5 vol.% $TiC_{0.7}N_{0.3}$ coated granule surface – high mag.

measurements were carried out by using the two probe method at room temperature on disc shape samples. To facilitate this measurement, Au electrodes were deposited on both sides of the samples.

3. Results and discussion

3.1. Efficiency of dry mixing process

SEM images taken from the surfaces of uncoated and coated granules under different magnification are presented in Fig. 1. Before the mixing process, the granules had a rough surface texture and the primary Si_3N_4 particles were clearly visible (Fig. 1a and b). After the mixing process, a relatively smooth granule surface covered with TiCN nano particles was observed as evidence of a successful coating process. Concurrently agglomerated nano TiCN particles were also observed (Fig. 1c and d). Although a simple mixing process was employed, the rough surface features of the granules aided the entrapment of nano TiCN particles on the surface during the mixing process. In addition, electrostatic attraction between the nano TiCN powders was thought to be effective in helping the formation of the homogenous coating.[28]

3.2. Phase and microstructural development

Comparative XRD patterns of the both composites were shown in Figs. 2 and 3. α-SiAlON, β-SiAlON and $TiC_{0.3}N_{0.7}$ were detected as the major crystalline phases. A small amount of in-situ SiC phase formation was observed in the SN-25 composite. Formation of SiC was also confirmed using SEM analysis. In Fig. 4, high magnification SEM images obtained from SN-25 and SNC-10 composites are shown. The possible in situ formed SiC grains are indicated by arrows on the images. In both composites, SiC grains appear to be formed around and/or along TiCN particles. The main reason for this formation is believed to be reaction between the TiCN and primary Si_3N_4 particles in accordance with the relevant work.[17,35] The Gibbs free energy

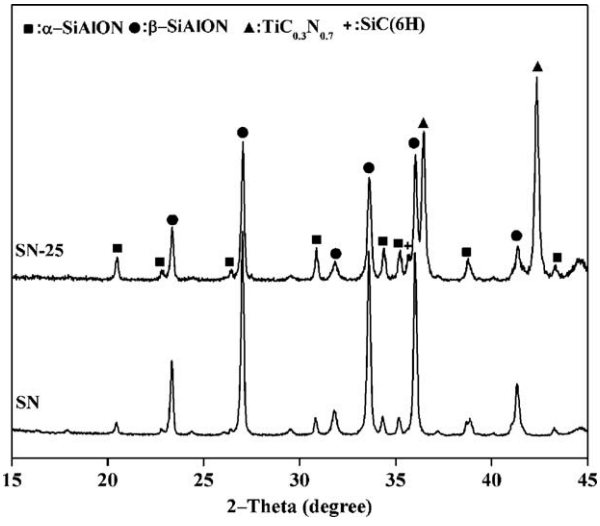

Fig. 2. XRD patterns of the matrix material (SN) and the TiCN particle reinforced composite (SN-25).

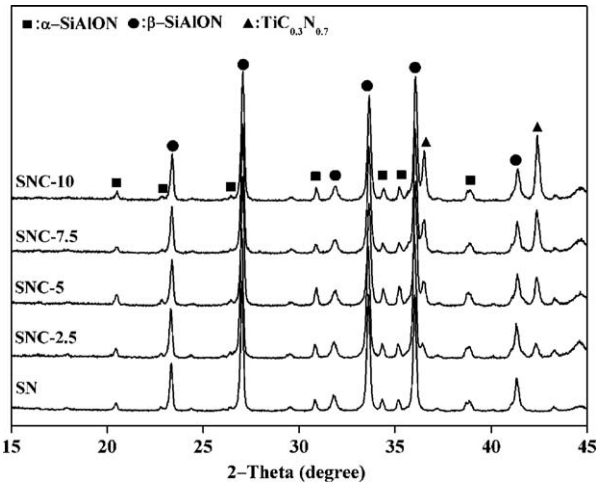

Fig. 3. XRD patterns of the matrix material (SN) and the SNC composites (SNC-2.5, SNC-5, SNC-7.5 and SNC-10).

of the possible reactions at the sintering temperature was evaluated using MTDATA (version 4.74) software and is given in reactions (2) and (3). Since the Ti(C, N) is a solid solution of TiC and TiN, the formation energy for $TiC_{1-x}N_x$ solid solutions can be calculated from Eq. (4) by means of varying the value of x.[35]

$$10TiC_{0.5}N_{0.5} + \frac{2}{3}Si_3N_4 \rightarrow TiC_{0.3}N_{0.7} + 2SiC + \frac{1}{2}N_2 \quad (2)$$

$$\Delta G^{\circ}{}_{1990^{\circ}C} = -103.71\ \text{kcal/mol}.$$

$$15TiC_{0.7}N_{0.3} + 2Si_3N_4 \rightarrow 15TiC_{0.3}N_{0.7} + 6SiC + N_2 \quad (3)$$

$$\Delta G^{\circ}{}_{1990^{\circ}C} = -332.42\ \text{kcal/mol}.$$

$$\Delta G^{o}_{TiC_{1-x}N_x} = xG^{o}_{TiC} + (1-x)\Delta G^{o}_{TiN} + RT[x\ \ln\ x + (1-x)\ln(1-x)] \quad (4)$$

Furthermore, the difference in the C:N ratio of the starting TiCN powders after sintering revealed that the C and N atoms may substitute with each other or dissolve into the liquid phase during sintering. As stated earlier, Ti(C, N) is a solid solution of TiC/TiN and it has a binary fcc crystal structure; with the atoms of carbon and nitrogen occupying all the octahedral interstitial sites.[36,37] The lattice parameter of TiC_xN_{1-x} solid solution is a linear function of the composition and fulfills Vegard's law.[38–40] Thus, the composition of TiC_xN_{1-x} was estimated from Vegard's law by using JCPDS data files: $TiC_{0.3}N_{0.7}$ (42–1488), TiN (38–1420) and TiC (32–1383) and the XRD patterns.[41] The compositions of the composites from the lattice parameters and the XRD measurements are given in Table 1. The calculated data confirm that C atoms from TiCN particles were substituted with N atoms or released during sintering, which may have led to the formation of SiC particles. It should also be noted that the high sintering temperature (1990 °C) required to achieve full densification in the composites investigated may also be another reason for the reactions between the constituent phases.

Table 1
Lattice parameter (a) and calculated compositions of TiCN phase after gas pressure sintering.

Sample	a (Å)	Composition calculated from XRD patterns
SN-25	4.2709	$TiC_{0.34}N_{0.66}$
SNC-2.5	4.2750	$TiC_{0.38}N_{0.62}$
SNC-5	4.2691	$TiC_{0.32}N_{0.68}$
SNC-7.5	4.2687	$TiC_{0.28}N_{0.72}$
SNC-10	4.2644	$TiC_{0.15}N_{0.85}$

The effect of TiCN addition on the α–β SiAlON phase ratio of the composites was also calculated from the XRD peak intensities using α [(1 0 2), (2 0 1)] and β [(1 0 1), (2 1 0)][33] characteristic peaks (Table 2). According to the results, incorporation of TiCN in the investigated SiAlON system tends to decrease the α → β SiAlON phase conversion in both types of the composites. The highest α:β phase ratio was observed in the SN-25 composite due to the high volume of the TiCN phase. Thus, small additions of TiCN also increase the α-SiAlON phase content in the SNC based composites. α–β SiAlON transformation during the sintering process is controlled by the dissolution and re-precipitation of particles from an intergranular liquid phase, as in the Si_3N_4 system.[42,43] The viscosity of the liquid phase determines the α → β conversion rate. This is thought to be due to the fact that the incorporation of Ti^{4+} and C^{4-} from the TiCN particles alters the viscosity of the liquid phase during sintering, and which plays a dominant role on the transformation of α → β

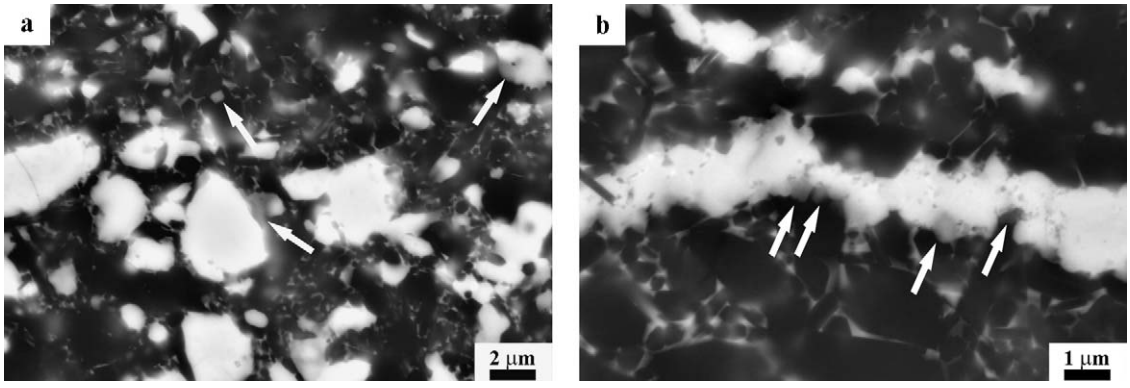

Fig. 4. SiC formation around TiCN particles is indicated with arrows: (a) SN-25 and (b) SNC-10. Bright grains indicate TiCN grains and the light gray colored formations around and/or along the TiCN particles indicate SiC grains formed in situ.

Table 2
Properties of the investigated composites.

Composition	Measured density (g/cm^3)	Relative density (%)	α/β phase ratio	Hv_{10} (GPa)	K_{IC} (MPa m$^{1/2}$)	Resistivity (Ω m)
SN	3.25	99.9	0.22	14.85 ± 0.14	5.86 ± 0.11	1×10^{13}
SN 25	3.68	98	0.53	18.87 ± 0.27	6.39 ± 0.19	0.45
SNC-2.5	3.28	99.9	0.25	14.87 ± 0.17	5.80 ± 0.06	9
SNC-5	3.35	99.9	0.33	14.95 ± 0.32	5.88 ± 0.12	18×10^{-4}
SNC-7.5	3.41	99.9	0.34	14.96 ± 0.29	5.92 ± 0.09	15×10^{-4}
SNC-10	3.45	99.9	0.34	15.01 ± 0.21	5.95 ± 0.07	13×10^{-4}

SiAlON. Relevant studies showed that incorporation of Ti^{4+} ions originating from the surface TiO_2 layer of TiCN particles decreased the viscosity of the liquid phase; however, incorporation of additional C^{4-} ions increased the viscosity of the liquid phase due to one bridging carbon assembling four structural units of glass together.[44] In the SN-25 composite, a high amount of TiCN (25 vol.%) addition affected the designed SiAlON composition such that higher amounts of α-SiAlON phase remained than expected under the selected sintering conditions.

Back scattered SEM images taken from the polished surfaces of the composites are given in Fig. 5. In the images, elongated grains with a dark grey color represent β-SiAlON; small

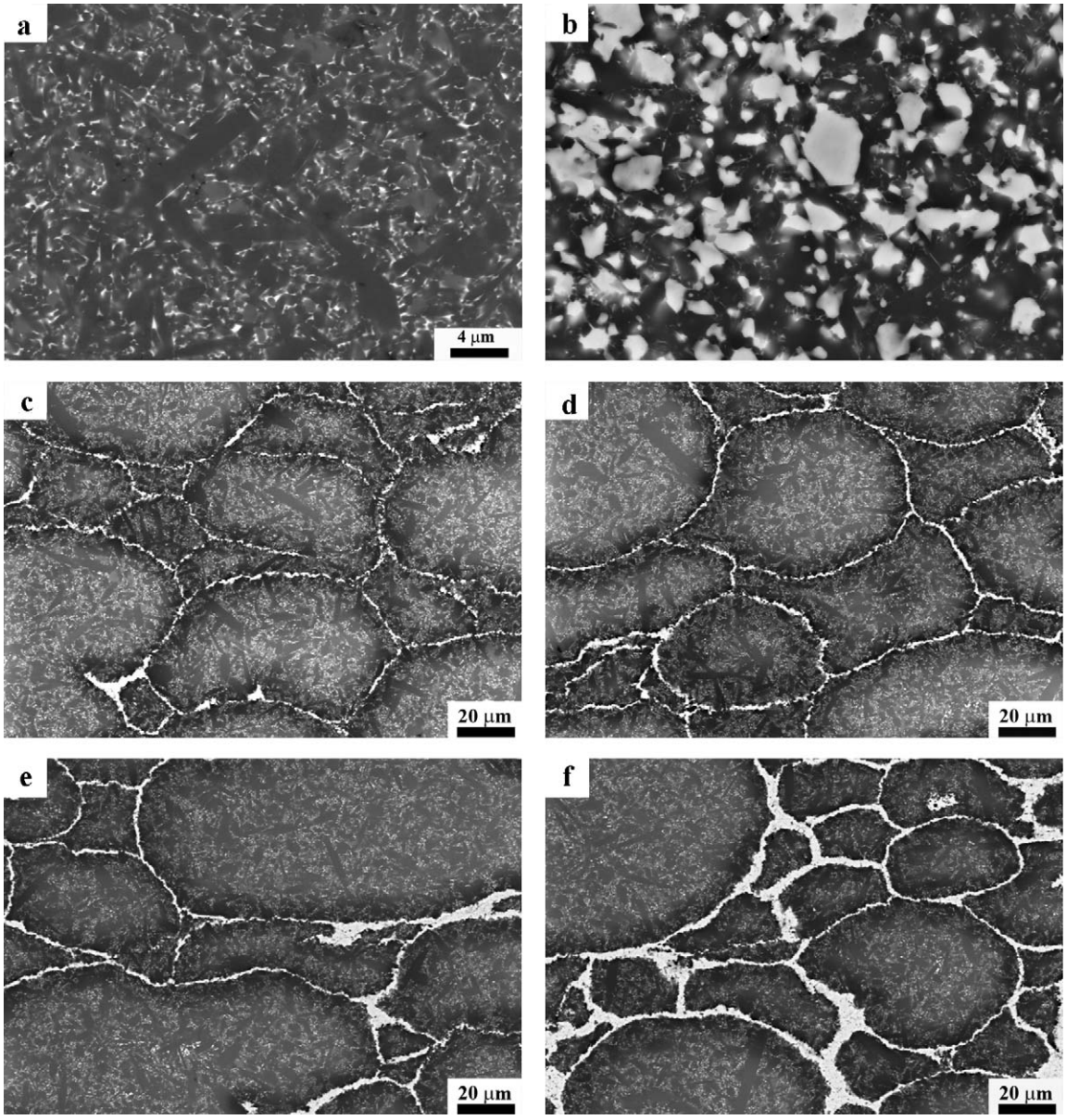

Fig. 5. SEM images of the polished surface of investigated composites. (a) SN, (b) SN-25, (c) SNC-2.5, (d) SNC-5, (e) SNC-7.5 and (f) SNC-10.

and equi-axed grains with light grey color represent α-SiAlON; grains with bright contrast represent TiCN grains. Formation of large elongated β-SiAlON grains was observed in the SN matrix due to the high sintering temperature and long holding time. Also, well dispersed but small α-SiAlON grains were located between β-SiAlON grains. In SN-25 composite, TiCN particles were homogenously dispersed in the matrix. When compared with the matrix material, β-SiAlON grains were not as large; indicating that introduction of large amounts of secondary phase limits the growth of the elongated grains as a result of the volume effect and pinning of the growth direction of the elongated particles.

The SEM images in Fig. 5c–f, demonstrate that it was possible to coat spray dried granules with nano particles by means of mechanical mixing and these could be densified using GPS. In all the composites, formation of a segregated network of nano TiCN particles was successfully achieved. With increasing amount of TiCN particles, the thickness of the coated layer increased accordingly. The large granules preserved their spherical starting shape but the small granules situated between the larger ones tended to be deformed. Internally, granules appeared to be sintered but isolate from each other. However, comparative SEM images with higher magnification taken from SNC-2.5 and SNC-10 composites (Fig. 6) revealed that due to the low coating thickness, granules were linked to each other during sintering. The significant increase in the electrical conductivity above 5 vol.% TiCN addition may be attributed to this linking phenomenon due to the interruption of the continuous network between conductive TiCN particles. Isolated granule boundaries tend to inhibit the grain growth of large β-SiAlON grains.

During the microstructural investigations of the SNC based composites, a contrast difference between the granule boundaries and the granule center was observed. Large β-SiAlON grains tended to form rather than α-SiAlON grains along these borders. Thus, the α–β SiAlON phase transformation was thought to have occurred more rapidly in these regions. Since no data is available for the oxygen content of the nano TiCN powder, it was believed that the incorporation of surface oxygen had decreased the liquid phase formation temperature and affected the viscosity of the liquid phase which consequently accelerated the α–β SiAlON phase transformation. Under examination in the SEM, β-SiAlON grains exhibit low atomic contrast rather than the multi-cation doped α-SiAlON grains and liquid phase and as a result, a contrast difference was observed.

3.3. Mechanical properties

Vickers hardness and the indentation fracture toughness of the composites are presented in Table 2. Mechanical properties of α–β SiAlON ceramics depend on the relative amounts, size and shape of the α and β SiAlON phases, in a similar manner to the Si_3N_4 ceramics. α-SiAlON grains are generally equi-axed in shape, as observed in the SEM images. This feature improves the hardness particularly due to the cations incorporated into the lattice structure such as Ca.[45] However, as a consequence of the shape factor, this feature decreases the fracture toughness of the material. β-SiAlON grains tend to be elongated in shape which acts similar to a whisker and thus increases the fracture toughness. It is possible to produce both hard and tough SiAlON ceramics by stabilizing both α and β structures in the same microstructure.[46,47]

Considering the α/β SiAlON ratio measured by means of X-ray peak intensities, it is clear that the hardness and toughness of the investigated composites were strongly affected. The particulate composite SN-25 possessed the highest amount of α-SiAlON phase and as a result it has considerably high hardness. In addition, the contribution of the hard and micron sized TiCN particles and the formation of in situ SiC particles is thought to be the reason for the improved hardness for this composite. The hardness of the matrix and the SNC based composites was found to be relatively lower than that of the SN-25 composite. One reason for this decrease could be the lower α-SiAlON content of both materials. Another possible reason is the size of β-SiAlON grains which affects the fracture modes. In the SEM images, it was clear that SN-25 contains thinner β-SiAlON grains when compared with both matrix and SNC based composites, which have moderate hardness values.

Fracture toughness of the composites is summarized in Table 2. The self reinforced matrix material (SN) and the composites prepared by coating granules (SNC) showed similar fracture toughness values of around 5.8 MPa $m^{1/2}$. The crack paths induced during the Vickers indentation are shown in Fig. 7. In SN and SNC-10, the crack propagation continued throughout the α-SiAlON and β SiAlON grains; thus a tortu-

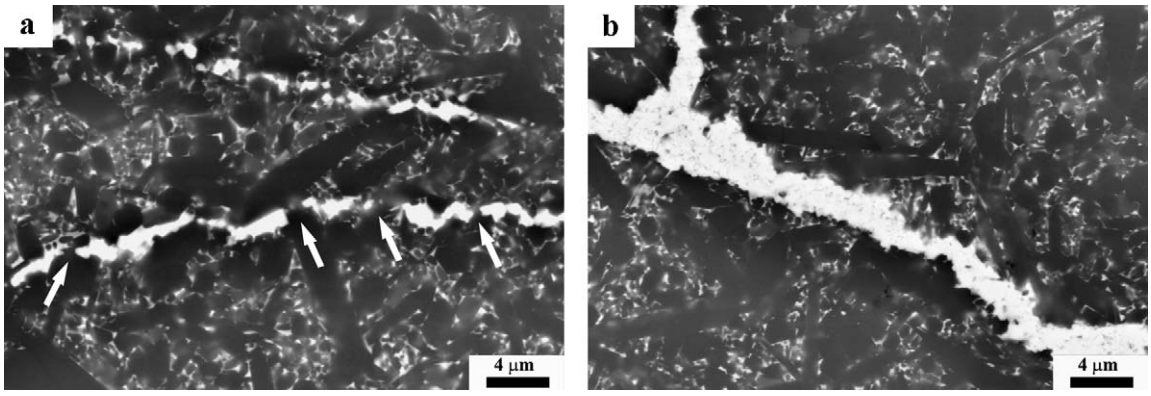

Fig. 6. High magnification SEM images of the composites: (a) SNC-2.5 and (b) SNC-10 showing the linking of granules due to the low coating thickness.

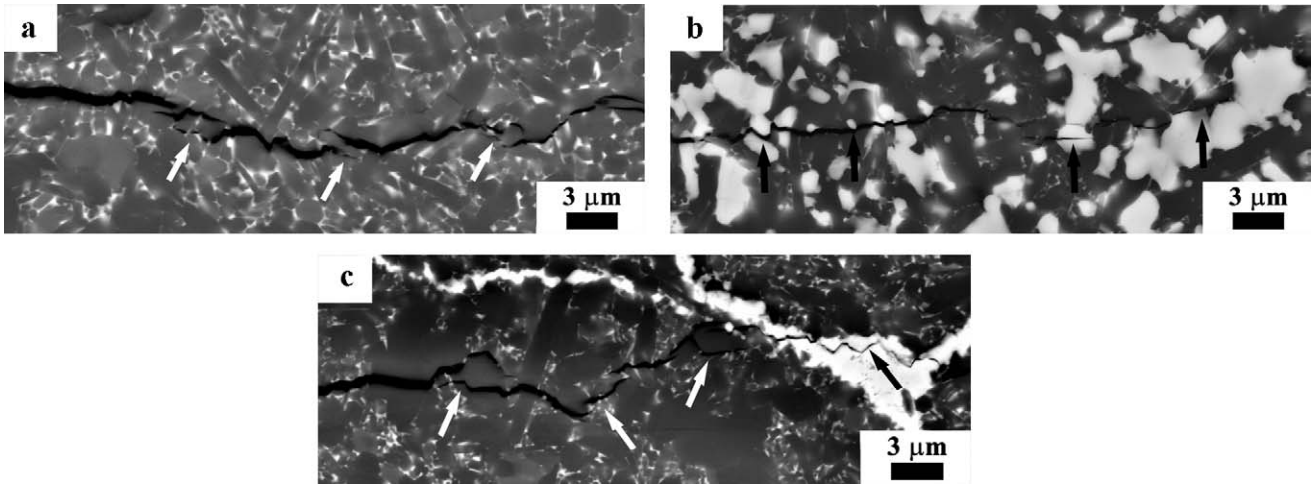

Fig. 7. SEM images depicting the crack paths originated during Vickers indentation (a) SN, (b) SN-25 and (c) SNC-10.

ous crack path was observed. Due to the interlocking nature of microstructural features, crack deflection, crack bridging and pull-out mechanisms contributed to the moderate toughness of these composites. In addition, crack deflection due to nano TiCN particles was visible in the images.

The fracture toughness increased with the incorporation of micron sized TiCN in SN-25 composite to a value of 6.39 MPa $m^{1/2}$. The cracking in the SN-25 composite tends to propagate by evading TiCN grains. Concurrently, crack bridging of randomly oriented small β-SiAlON grains contributes to the toughness. Due to the thermal mismatch effect between the matrix ($\alpha_{matrix} = 3.2 \times 10^{-6}\ K^{-1}$) and the TiCN ($\alpha_{particle} = 8.6 \times 10^{-6}\ K^{-1}$) along with the presence of TiCN particles, radial residual tensile stresses are believed to be formed.[48] The stress interference stripes in the matrix which resulted during cooling during the sintering process are indicated by the arrows in Fig. 8. The stripes generally formed in the areas where pull-out of TiCN grains took place.

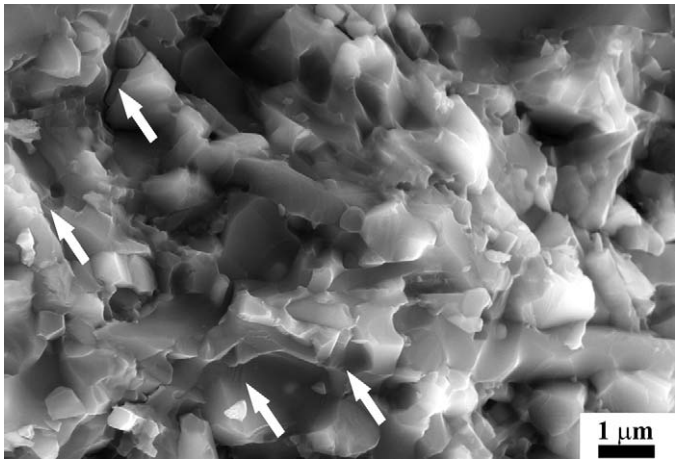

Fig. 8. SEM image taken from the fracture surface of the SN-25 composite. The arrows indicate the stress interference stripes in the SN matrix where TiCN particles have been pulled out during fracture.

3.4. Electrical properties

The electrical resistivity values of the composites are given in Table 2 and also plotted as a function of the TiCN content in Fig. 9. The electrical resistivity of monolithic SN material is 10^{13}–10^{14} Ω m, which is in the range expected from an insulator. The resistivity of the SN material substantially decreased in the SNC based composites. With this coating process, the percolation threshold value was found to be as low as 2.5 vol.% TiCN addition with a resistivity value of 5.2 Ω. The resistivity value was further decreased down to 18×10^{-4} Ω m with 5 vol.% TiCN. However, increasing the TiCN amount over 5 vol.% did not cause any further improvement. This indicates that above 5 vol.% TiCN, conductivity was enabled by the physical contact of TiCN particles in three dimension, which was also confirmed by the microstuctural investigation (Fig. 6).

SN-25 composite showed a resistivity value of 0.45 Ω m. Considering the microstructure of this composite, due to the random distribution of conductive TiCN particles, both particle contact and tunneling conduction mechanisms are thought

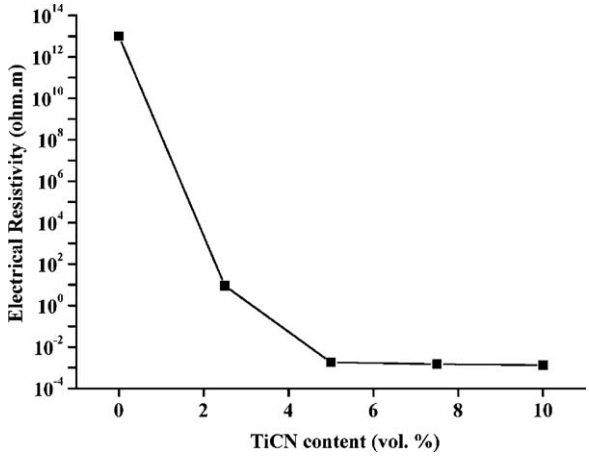

Fig. 9. Change in the electrical resistivity of SNC based composites with TiCN content.

to be taken place concurrently. As mentioned earlier, low levels of $\alpha \rightarrow \beta$ conversion during the sintering process inhibits the amount and the size of the β-SiAlON grains in the SN-25 composite. The distance between TiCN particles was decreased with the formation of small β-SiAlON grains. This phenomenon is thought to aid the tunneling conduction mechanism between TiCN particles that enhances electrical conductivity. Thus, in terms of the conductivity of this composite, the value was found to be near the percolation threshold value for the particle reinforced composite systems.

4. Conclusions

Electrically conductive α–β SiAlON–TiCN composites were produced by means of a segregated network concept. With the dry mixing process, spray dried SiAlON based granules ($\leq$100 μm) were coated with varying amounts of (up to 10 vol.%) nano TiCN ($\leq$150 nm) particles. For comparison a particle reinforced composite containing 25 vol% micron sized TiCN was prepared. All the composites investigated and the reference SiAlON material were fully densified with gas pressure sintering at 1990 °C under a N_2 gas pressure of 10 MPa. A chain type 3D microstructure to establish electrical conductivity in the composites was successfully achieved with incorporation of only 2.5 vol.% TiCN. The electrical resistivity of the insulator SN material ($\sim 10^{13}$ Ω m) was decreased drastically to a value of 18×10^{-4} Ω m with the addition of 5 vol.% TiCN nano particles.

XRD analysis and thermodynamic investigation proved that TiCN and Si_3N_4 particles reacted with each other during sintering. Thus in both types of composites, in situ SiC grains appears to be formed around and/or along TiCN particles. In particle reinforced composite (SN-25) the $\alpha \rightarrow \beta$ SiAlON phase transformation was strongly affected by these reactions. The incorporation of significant amounts of surface O and substitution of C and N in the liquid phase altered the phase transformation and intragranular phase formation, which influenced the mechanical properties of the SN matrix. No significant changes in the mechanical properties were observed for the SNC based composites.

Acknowledgements

The authors would like to thank to Anadolu University/TURKEY Research Foundation for funding the present work under a contract number of 60266 and also MDA Advanced Ceramics Ltd., Eskişehir/Turkey for supplying the spray-dried SiAlON granules.

References

1. Riley F. Silicon nitride and related materials. *J Am Ceram Soc* 2000;**83**(2):245–65.
2. Gogotsi YG. Particulate silicon nitride based composites. *J Mater Sci* 1994;**29**:2541–56.
3. Martin C, Cales B, Viver P, Mathieu P. Electrical discharge machinable ceramic composites. *Mater Sci Eng A* 1989;**109**:351–6.
4. Lok YK, Lee TC. Processing of advanced ceramics using the wire cut EDM process. *J Mater Process Tech* 1997;**63**:839–43.
5. Liu CC, Huang JL. Micro-electrode discharge machining of TiN/Si_3N_4 composites. *Br Ceram Trans* 2000;**99**(4):149–52.
6. Bellosi A, Guicciardi S, Tampieri A. Development and characterization of electroconductive Si_3N_4–TiN composites. *J Eur Ceram Soc* 1992;**9**(2):83–93.
7. Boskovic S, Sigulinski F, Zivkovic L. Liquid phase sintering and properties of Si_3N_4–TiN composites. *J Mater Synt Process* 1999;**7**(2):119–26.
8. Zivkovic L, Nikolic Z, Boskovic S. Electrical properties and percolation concentration in Si_3N_4–TiN based composites. *Euro Ceram VII* 2002;**206-2**(Pt 1–3):1489–92.
9. Zhiquan G, Gurdial B, Reneĭ K, Mike R, Thomas G, Jakob K. Microstructure and electrical properties of Si_3N_4–TiN composites sintered by hot pressing and spark plasma sintering. *Ceram Int* 2007;**33**(7):1223–9.
10. Sawaguchi A, Toda K, Niihara K. Mechanical and electrical properties of silicon nitride-silicon carbide nanocomposite material. *J Am Ceram Soc* 1991;**74**(5):1142–4.
11. Kim WJ, Taya M, Yamada K, Kamiya N. Percolation study on electrical resistivity of SiC/Si_3N_4 composites with segregated distribution. *J Appl Phys* 1998;**83**(5):2593–8.
12. Yamada K, Kamiya N. High temperature mechanical properties of Si_3N_4–$MoSi_2$ and Si_3N_4–SiC composites with network structures of second phase. *Mater Sci Eng A* 1999;**261**:270–7.
13. Petrovsky VY, Rak RZ. Densification, microstructure and properties of electroconductive Si_3N_4–TaN composites. Part II. Electrical and mechanical properties. *J Eur Ceram Soc* 2001;**21**:237–44.
14. Kao MY. Properties of silicon nitride-molybdenum disilicide particulate ceramic composites. *J Am Ceram Soc* 1993;**76**(11), 2879-2875.
15. Sciti D, Guicciardi S, Bellosi A. Microstructure and properties of Si_3N_4–$MoSi_2$ composites. *J Ceram Process Res* 2002;**3**(3):87–95.
16. Guo ZQ, Blugan G, Graule T. The effect of different sintering additives on the electrical and oxidation properties of Si_3N_4–$MoSi_2$ composites. *J Eur Ceram Soc* 2007;**27**(5):2153–61.
17. Hermann M, Blazer B, Schubert Chr, Hermel W. Densification, microstructure and properties of Si_3N_4–Ti(C, N) composites. *J Eur Ceram Soc* 1993;**12**:287–96.
18. Jiang DT, Vleugels J, Van Der Biest O, Liu W, Verheyen R, Lauwers B. Electrically conductive and wear resistant Si_3N_4-based composites with $TiC_{0.5}N_{0.5}$ particles for electrical discharge machining. *Mater Sci Forum* 2005;**492–493**:27–32.
19. Jones AH, Trueman C, Dobedoe RS, Huddleston J, Lewis MH. Production and EDM of Si_3N_4–TiB_2 ceramic composites. *Br Ceram Trans* 2001;**100**:49–54.
20. Gao L, Li J, Kusunose T, Niihara K. Preparation and properties of TiN–Si_3N_4 composites. *J Eur Ceram Soc* 2004;**24**(2):381–6.
21. Kawano S, Takahashi J, Shimada S. The preparation and spark plasma sintering of silicon nitride-based materials coated with nano-sized TiN. *J Eur Ceram Soc* 2004;**24**:309–12.
22. Krnel K, Maglica A, Kosmac T. β-SiAlON/TiN nanocomposites prepared from TiO_2-coated Si_3N_4 powder. *J Eur Ceram Soc* 2008;**28**:953–7.
23. Bouchet J, Carrot C, Guillet J, Boiteux G, Seytre G, Pineri M. Conductive composites of UHMWPE and ceramics based on the segregated network concept. *Poly Eng Sci* 2000;**40**:36–45.
24. Sandler JKW, Kirk JE, Kinloch IA, Shaffer MSP, Windle AH. Ultra-low electrical percolation threshold in carbon nanotube–epoxy composites. *Polymer* 2003;**44**:5893–9.
25. Carmona F. Conducting filled polymers. *Physica A* 1989;**157**:461–9.
26. Kirkpatrick S. Percolation and conduction. *Rev Mod Phys* 1973;**45**(4): 574–88.
27. McLachlan DS, Blaszkiewicz M, Newnham RE. Electrical resistivity of composites. *J Am Ceram Soc* 1990;**73**(8):2187–203.
28. Kusy RP. Influence of particle size ratio on the continuity of aggregates. *J Appl Phys* 1977;**48**(12):5301–5.
29. Friedman H, Donbrow M, Samuelov Y. Release rate of drugs from ethyl cellulose coated granules containing caffeine and salicylic acid. *Drug Develop Ind Pharm* 1979;**5**(4):407–24.
30. Teunou E, Poncelet D. Batch and continuous fluid bed coating—review and state of the art. *J Food Eng* 2002;**53**:325–40.

31. Guignon B, Duquenoy A, Dumoulin ED. Fluid bed encapsulation of particles: principles and practice. *Dry Tech* 2002;**20**(2):419–47.
32. Mandal H, Kara F, Turan S, Kara A, US Patent No: US 7,064,095, 2002.
33. Gazzara CP, Messier DR. Determination of phase content of Si_3N_4 by X-ray diffraction analysis. *Ceram Bull* 1977;**56**:777.
34. Evans AG, Charles EA. Fracture toughness determination by indentation. *J Am Ceram Soc* 1976;**59**(7):371–2.
35. Jiang DT, Vleugels J, Van Der Biest O. Development and characterization of SiAlON composites with TiB_2, TiN, TiC and TiCN. *J Mater Sci* 2004;**39**:3375–81.
36. Pastor H. Titanium-carbonitride-based hard alloys for cutting tools. *Mater Sci Eng A* 1988;**106**:401–9.
37. Levi G, Kaplan WD, Bamberger M. Structure refinement of titanium carbonitride (TiCN). *Mater Lett* 1998;**35**:344–50.
38. Alekseev NV, Samokhin AV, Tsvetkov YV. Synthesis of titanium carbonitride nano powder by titanium tetrachloride treatment in hydrocarbon-plasma. *High Energy Chem* 1999;**33**:194–7.
39. Wokulska K. Thermal expansion of whiskers of Ti(C, N) solid solutions. *J Alloy Compd* 1998;**264**:223–7.
40. Kerr A, Welham NJ, Willis PE. Low temperature mechanochemical formation of titanium carbonitride. *Nanostruct Mater* 1999;**11**:233–9.
41. Denton AR, Ashcroft NW. Vegard's law. *Phys Rev A* 1991;**43**:3161–4.
42. Cao GZ, Metselaar R. α-SiAlON ceramics: a review. *Chem Mater* 1991;**3**:242–52.
43. Mandal H, Thompson DP, Ekstrom T. Reversible α ↔ β SiAlON transformation in heat-treated sialon ceramics. *J Eur Ceram Soc* 1993;**12**:421–9.
44. Duan RG, Roebben G, Vleugels J, Van der Biest O. Effect of TiX (X = C, N, O) additives on microstructure and properties of silicon nitride based ceramics. *Scripta Mater* 2005;**53**:669–73.
45. Mandal H, Hoffman MJ. Hard and tough α-SiAlON ceramics. *Mater Sci Forum* 2000;**325-326**:219–24.
46. Ekstrøm T, Nygren M. SiAlON Ceramics. *J Am Ceram Soc* 1992;**75**(2):259–76.
47. Mandal H, Thompson DP. In: Galassi C, editor. *Mechanism for α ↔ β-SiAlON transformation; fourth euro-ceramics, developments in processing of advanced ceramics. PN Gruppo Editoriale Faenze Editrice SpA*, vol. 2. 1995. p. 327–444.
48. Zhao J, Ai X, Lü Z. Preparation and characterization of Si_3N_4/TiC nanocomposite ceramics. *Mater Lett* 2006;**60**:2810–3.